Controlling Shape Anisotropy of ZnS-$AgInS_2$ Solid Solution Nanoparticles for Improving Photocatalytic Activity

Tsukasa Torimoto,[1] Yutaro Kamiya,[1] Tatsuya Kameyama,[1] Hiroyasu Nishi,[2] Taro Uematsu,[3] Susumu Kuwabata,[3] and Tamaki Shibayama[4*]*

[1]Graduate School of Engineering, Nagoya University, Nagoya 464-8603, Japan,

[2]Institute of Industrial Science, The University of Tokyo, Tokyo 153-8505, Japan

[3]Graduate School of Engineering, Osaka University, Suita, Osaka 565-0871, Japan

[4]Center for Advanced Research of Energy Conversion Materials, Hokkaido University, Sapporo 060-8628, Japan

KEYWORDS Semiconductor nanoparticle, Quantum dot, Multinary metal sulfide, Solid solution, Anisotropic crystal growth, Photocatalyst

ABSTRACT

Independently controlling the shape anisotropy and chemical composition of multinary semiconductor particles is important for preparing highly efficient photocatalysts. In this study, we prepared ZnS-$AgInS_2$ solid solution ($(AgIn)_xZn_{2(1-x)}S_2$, ZAIS) nanoparticles with well-controlled anisotropic shapes, rod and rice shapes, by reacting corresponding metal acetates with a mixture of sulfur compounds with different reactivities, elemental sulfur and 1,3-dibutylthiourea, via a two-step heating-up process. The chemical composition predominantly determined the energy gap of ZAIS particles: the fraction of Zn^{2+} in rod-shaped particles was tuned by the ratio of metal precursors used in the nanocrystal formation, while post-preparative Zn^{2+} doping was necessary to increase the Zn^{2+} fraction in the rice-shaped particles. The photocatalytic H_2 evolution rate with irradiation to ZAIS particles dispersed in an aqueous solution was significantly dependent on the chemical composition in the case of using photocatalyst particles with a constant morphology. In contrast, photocatalytic activity at the optimum ZAIS composition, *x* of 0.35~0.45, increased with particle morphology in the order of rice (size: ca. 9 × ca.16 nm) < sphere (diameter: ca. 5.5 nm) < rod (size: 4.6 × 27 nm). The highest apparent quantum yield for photocatalytic H_2 evolution was 5.9% for rod-shaped ZAIS particles, being about two-times larger than that obtained with spherical particles.

INTRODUCTION

Controlling dimensions of nanomaterials has been a promising strategy to develop novel functionality and to improve their performance for various applications, such as photoluminescent devices, biomolecule markers, solar cells and photocatalysts, because the physicochemical properties are remarkably varied by both the degree of electron confinement in materials and the change in electron transport property to other materials.[1-9] Since procedures for the synthesis of high-quality binary semiconductor nanoparticles have been well established, most studies have been carried out with binary particles to determine the correlations of particle size and shape with physicochemical properties of the particles. For example, it was found that photo-functionalities of II-VI group semiconductor nanoparticles could be improved by control of their shape anisotropy. Rod-shaped CdSe particles were used for the fabrication of quantum dot-polymer hybrid solar cells, in which the conversion efficiency was improved with an increase in rod length.[2] The three-dimensional structure of tetrapod-shaped CdTe particles increased the number of electron transport paths across the light absorption layer of hybrid solar cells compared to that in the case of the one-dimensional structure of rod-shaped particles.[4] Photocatalytic activity of multi-armed CdS rod particles was higher than that of spherical or non-branched rod particles.[10] A change in the ratio of {0001} to {10-11} facets exposed on nanocrystals with a wurtzite structure resulted in a change in the anisotropic shape of the particles from a cone shape to a plate shape, and plate-like CdS particles with the largest {0001} facet showed the highest photocatalytic activity for H_2 evolution.[11]

On the other hand, much interest has recently been shown in multinary metal chalcogenide semiconductor particles as light-absorbing materials for solar cells and photocatalyts[12-24] because of their physicochemical properties that are tunable by their chemical composition and their low

toxicity compared to that of conventional binary semiconductors such as CdSe, CdTe and PbS. Spherical multinary nanoparticles of Cu_2ZnSnS_4 and $Cu(In,Ga)(S,Se)_2$ were synthesized by solution phase methods[14-16, 21, 23] and used as precursors for the fabrication of thin-film solar cells.[13-14, 16, 18] Sensitized quantum dot solar cells were successfully prepared by immobilizing spherical nanoparticles of a Zn-Cu-In-Se quaternary semiconductor on porous metal oxide electrodes, and solar energy conversion efficiency as high as ca. 11% was achieved.[25] Furthermore, visible-light-driven photocatalytic reactions, such as H_2 evolution[24, 26-31] and degradation of an organic dye,[32-34] have been intensively investigated using multinary semiconductor nanoparticles. We carried out photocatalytic H_2 evolution with spherical ZnS-$AgInS_2$ solid solution nanoparticles as a photocatalyst, the activity being controlled by particle size and chemical composition.[29]

Recent progress in solution phase syntheses has enabled multinary nanoparticles with anisotropic shapes, such as rod, arrow, tetrapod, disc and seed shapes, to be produced by controlling the reaction conditions,[35-42] and studies have been carried out to clarify their shape-dependent photocatalytic activities.[24, 27, 30, 33] Cabot et al. reported that the incorporation of Ga into bullet-like $CuInS_2$ particles resulted in a decrease in the length of particles but improvement in the photocatalytic H_2 evolution rate, the maximum activity being obtained with the composition of $CuIn_{0.3}Ga_{0.7}S_2$.[27] Han and co-workers reported that rod-shaped particles of ZnS-$CuInS_2$ solid solution (ZnS:$CuInS_2$=10:1) showed higher photocatalytic H_2 evolution activity than that of $CuInS_2$ rods.[30] Recently, we successfully prepared wurtzite-type Cu_2ZnSnS_4 nanorods via a two-step heat treatment procedure at 200 °C and 240 °C, in which the aspect ratio of particles could be varied by the ratio of individual sulfur compounds used as precursors.[43] As demonstrated in previous studies,[12, 13, 21, 24, 27, 30] the chemical composition has been clarified to be the primary parameter for determining the photocatalytic properties of multinary semiconductors. In addition,

by analogy with Cd-based binary nanoparticles, control of the particle morphology of multinary semiconductors is expected to be another significant parameter in designing multinary nanoparticles with controlled functional properties. However, accurate assessment of their shape-dependent photocatalytic activity remains a challenge because independent control of the morphology and chemical composition of multinary semiconductor particles, especially those consisting of four or more elements, has been difficult owing to the considerable difference in reactivities of precursors for individual elements.[21, 24, 27, 30, 33, 44-45]

Here, we report independent control of the particle shape and chemical composition for ZnS-$AgInS_2$ solid solution ($(AgIn)_xZn_{2(1-x)}S_2$, ZAIS) nanoparticles. Two-step heat treatment of precursor solutions, in which corresponding metal acetates reacted with a mixture of sulfur compounds, resulted in the production of rod-shaped and rice-shaped particles. The absorption properties could be controlled, without remarkable modification of the individual particle morphology, by changing the chemical composition. The ZAIS nanoparticles were suitable materials for clarifying shape- and composition-dependent photocatalytic activities.

EXPERIMENTAL SECTION

Materials

Oleylamine (OLA) was purchased from Tokyo Chemical Industry, and indium(III) acetate was obtained from Aldrich. Zinc(II) acetate, 1-dodecanethiol (DDT), 1,3-dibutylthiourea (DBTU), and elemental sulfur were purchased from Wako Chemicals. Other chemicals were supplied by Kishida Reagents Chemicals. All reagents were used as received. Aqueous solutions were prepared with purified water just before use by a Millipore Milli-Q system.

Syntheses of anisotropic-shaped ZAIS nanoparticles having rod and rice shapes

Anisotropic-shaped ZAIS nanoparticles were prepared by reacting corresponding metal acetates with a mixture of sulfur compounds with different reactivities, elemental sulfur and DBTU, via a two-step heating-up process, the strategy being modified from that used for Cu_2ZnSnS_4 nanorod preparation in our previous study.[43] A typical procedure is described below. Metal precursor powders of $Ag(CH_3COO)$, $In(CH_3COO)_3$, and $Zn(CH_3COO)_2$ with a mole ratio of x_p: x_p:2(1- x_p) (total metal ions: 0.20 mmol) were put into a test tube with a 2.5 cm^3 portion of OLA and 0.50 cm^3 portion of DDT as a surface modification agent, where x_p is used to denote the molar ratio of individual metal ions in precursors used. The suspension was heated at 150 °C with vigorous stirring under an N_2 atmosphere to yield a homogeneous transparent solution. To the solution, a 0.30 cm^3 portion of DDT solution, in which S (0.050 mmol) and DBTU (0.15 mmol) were dissolved at 90 °C, was swiftly added, followed by stirring for 30 min at 150 °C (first heating step). Then the reaction temperature was quickly raised to 250 °C with a rate of ca. 1.2 °C s^{-1} and the solution was further stirred for 0~10 min (second heating step). After cooling down to room temperature, the thus-obtained suspension was subjected to centrifugation at 4000 rpm for 5 min. The precipitates composed of ZAIS particles having rod and rice shapes were washed with methanol several times and then re-dissolved in chloroform (3.0 cm^3), followed by removal of large precipitates by centrifugation.

When the second heat treatment at 250 °C was carried out for 5 min or less, the obtained particles in most cases contained only rod-shaped ZAIS particles, but prolonged heating for more than 5 min resulted in the production of a mixture of particles including rod-shaped and rice-shaped

particles. In the latter case, the size-selective precipitation technique was used for separation of particles with individual shapes from as-prepared crude particles. A portion of methanol as a non-solvent, typically ca. 0.05-0.1 cm^3, was added to the chloroform solution (3.0 cm^3) containing as-prepared particles, followed by centrifugation to isolate the precipitates containing enriched ZAIS particles with a rod shape. The resulting supernatant was vacuum-evaporated to obtain ZAIS particles containing a larger fraction of rice-shaped particles. Thus-obtained ZAIS particles were again dissolved in a 3.0 cm^3 portion of chloroform. By applying these procedures several times, particles with only one shape, rod shape or rice shape, were isolated.

The chemical composition of ZAIS particles was determined by X-ray fluorescence spectroscopy (Rigaku, EDXL-300) or energy dispersive X-ray spectroscopy (EDS) analysis using a Hitachi SU-1500 scanning electron microscope equipped with an EDS analyzer (Horiba, Emax Energy EX-250). We experimentally determined the x value in the chemical formula of $(AgIn)_xZn_{2(1-x)}S_2$, based on elemental analysis of the obtained ZAIS particles. The obtained x value of anisotropic-shaped ZAIS particles was not always equal to the x_p value in preparation.

Composition control of rice-shaped ZAIS particles with Zn^{2+} doping

Rice-shaped ZAIS particles prepared with x_p= 0.90 according to the above-mentioned procedure were used as starting nanoparticles. A 10-mg portion of rice-shaped particles was dispersed in OLA (2.0 cm^3). After addition of the desired amount of $Zn(CH_3COO)_2$, the solution was heat-treated at 250 °C for 10 min with vigorous stirring under an N_2 atmosphere, followed by cooling down to room temperature. The degree of Zn^{2+} doping was controlled by the molar ratio of $Zn(CH_3COO)_2$ added to OLA to that of total metal ions contained in ZAIS particles used,

denoted as R_{Zn}, which was varied from 0 to 2.5 in the present study. The thus-obtained suspension was subjected to centrifugation. The resulting precipitates were washed with methanol several times and then re-dissolved in chloroform (3.0 cm^3), followed by removal of large precipitates by centrifugation.

Spherical ZAIS particles with various solid solution compositions

Spherical ZAIS particles were prepared with a single-step heating process according to our previous procedure.[29] Briefly, powders of corresponding metal acetates with a mole ratio of Ag:In:Zn = x_p: x_p:2(1- x_p) (total metal ions: 0.20 mmol) were put into a test tube with thiourea powder (0.20 mmol). After adding a mixture solution of OLA (2.95 cm^3) and DDT (0.05 cm^3), the solution was heated at 250 °C for 10 min with vigorous stirring under an N_2 atmosphere. The resulting solution was cooled to room temperature, and then large aggregated particles were removed from the solution by centrifugation. ZAIS particles were isolated from the supernatant by precipitation with the addition of methanol, followed by centrifugation. The thus-obtained precipitates were washed with methanol several times and then re-dissolved in chloroform (3.0 cm^3). The experimentally determined metal ratio of Ag:In:Zn in spherical ZAIS particles agreed well with those of precursors used in the preparation, but the value of x in the formula of $(AgIn)_xZn_{2(1-x)}S_2$ was obtained on the basis of results of elemental analysis. TEM measurement revealed that thus-obtained ZAIS particles were spherical particles regardless of the x value, the average size of which was ca. 5.5 nm.

Characterization of ZAIS particles

The size distribution of nanocrystals was determined with a transmission electron microscope (TEM, Hitachi, H-7650) at an operation voltage of 100 kV. Samples for TEM measurements were prepared by dropping a particle-containing chloroform solution onto a copper TEM grid covered with an amorphous carbon overlayer (Okenshoji Co., Ltd, ELS-C10, STEM Cu100P grid), resulting in drying under vacuum. High-resolution transmission electron microscopy (HRTEM) images were taken by using a transmission electron microscope (JEM-2010F, JEOL, Japan) with a Schottky thermal field emission gun (FEG) operating at 200 kV. A fast Fourier transform (FFT) pattern of each image was obtained by using software (Gatan Microscopy Suite, Digital Micrograph, Gatan Inc., USA). The crystal structure was determined by measuring the powder X-ray diffraction (XRD) pattern with a Rigaku Smart-Lab using Cu Kα radiation.

UV-visible absorption spectra were obtained with a spectrophotometer (Agilent Technology 8453A). Photoluminescence (PL) spectra were measured with an excitation wavelength of 365 nm by using a photonic multichannel analyzer (HAMAMATSU, PMA-12). PL decay curves at room temperature were recorded by a time-correlated single-photon counting apparatus (HAMAMATSU, Quantaurus-Tau) equipped with photodiodes. The samples used for absorption and PL spectra were ZAIS particles uniformly dispersed in chloroform.

Shape- and composition-dependent photocatalytic H_2 evolution of ZAIS nanoparticles

ZAIS particles with anisotropic shapes were dissolved in toluene, followed by refluxing for 1 h to remove excess amounts of OLA and DDT adsorbed. After cooling the solution, ZAIS particles were again isolated with the addition of methanol and washed several times with methanol and one time with 2-propanol, followed by dispersion of the wet precipitates in 2-propanol by

ultrasonication for 5 min. The thus-obtained ZAIS nanoparticles (total metal ions: 4.5 μmol) were dispersed in a 5.0-cm^3 portion of water/2-propanol (1:1) mixture solution containing 50 mmol dm^{-3} Na_2S, in which both 2-propanol and sulfide ion acted as hole scavengers. The suspension was deaerated with Ar bubbling for 30 min and then irradiated by a 300-W Xe lamp (λ> 350 nm) under an Ar atmosphere with vigorous magnetic stirring at room temperature. The light intensity used for irradiation was 500 mW cm^{-2}. The amount of H_2 evolved was measured by an Agilent micro-GC 3000A gas chromatograph equipped with a molecular sieve 5A column. Apparent quantum yield was obtained by irradiation of monochromatic light with a wavelength of 400 nm (light intensity: 25.6 mW cm^{-2}), which was extracted from a Xe lamp light through an interference filter, to the same suspension except for increasing the amount of ZAIS particles added by 10 times to completely absorb the irradiated monochromatic light.

RESULTS AND DISCUSSION

Preparation of ZAIS particles with anisotropic shapes via a two-step heating process

Anisotropic-shaped ZAIS nanoparticles were prepared by reacting corresponding metal acetates with a mixture of sulfur compounds with different reactivities, elemental sulfur and DBTU, via a two-step heating-up process, the strategy being modified from that used for Cu_2ZnSnS_4 nanorod preparation in our previous study.[43] The first heating step at 150 °C changed the oleylamine solution from colorless to dark brown. The solution was immediately subjected to the second heating step at 250 °C, resulting in further change in the color of the solution to red or reddish brown. The size and shape of particles prepared with x_p = 0.50 were clarified by TEM measurements as shown in **Figure 1**, where x_p represent the molar fractions of $Ag(CH_3COO)$ and

$In(CH_3COO)_3$ in the metal precursor used in the preparation, Ag:In:Zn = x_p: x_p:2(1- x_p). Spherical particles were produced after the first heat treatment at 150 °C, the size distribution of which was relatively narrow with a diameter of 4.6±0.65 nm. These particles exhibited a broad XRD pattern assignable to be a cubic Ag_2S crystal structure (**Fig. S1a**), and their chemical composition was determined to be Ag:In:Zn:S = 56 : 1.0 : 1.8 : 41, suggesting that small amounts of Zn^{2+} and In^{3+} were doped into Ag_2S nanocrystals. The second heat treatment at 250 °C induced anisotropic particle growth without enlargement of the spherical particles. Rod-shaped particles were newly evolved with heating for 1.5 min (**Fig. 1b**). The rod-shaped particles had a length of 12±5.1 nm and width of 5.3±1.7 nm, though spherical Ag_2S particles of similar size, produced at the first heating step, were still observed. It should be noted that some of the rod particles had a spherical Ag_2S particle, exhibiting darker contrast, on their tip as shown in the inset of **Fig. 1b**. This suggested that the crystal growth of rod particles occurred on spherical Ag_2S particles. With prolongation of the second heating step to 3 min, spherical Ag_2S particles completely disappeared and rod-shaped particles were exclusively observed (**Fig. 1c**). The Ag_2S particles were probably re-dissolved into the solution and/or acted as a sacrificial source for crystal growth of rod-shaped particles. The length of thus-obtained rod particles increased to 40±10 nm from that observed after heating for 1.5 min, 12±5.1 nm, while the rod width was 5.3±0.98 nm, being almost unchanged regardless of heating time. XRD patterns of thus-obtained rod particles shown in **Fig. S1b** agreed well with those expected from the hexagonal wurtzite crystal structure of ZnS-$AgInS_2$ solid solutions.[12]

In contrast, prolongation of heating in the second step at 250 °C to 10 min resulted in the production of another kind of particle as a by-product. The particles had darker contrast with an anisotropic shape resembling a grain of rice as shown in a TEM image (**Fig. 1d**). Measurement of

the dimensions of the rice-shaped particles in the image showed that the particles had a width and length of 9.2±2.2 nm and 18±2.5 nm respectively, while little change was observed in the sizes of rod-shaped particles prepared with the second heating step for 3 to 10 min. The number ratio of rod particles : rice particles was 76 : 24. The XRD pattern of this particle mixture (**Fig. S1c**) contained additional peaks that were not assignable to rod-shaped ZAIS particles, indicating that rice-shaped particles had a lattice constant different from that of rod particles.

Size-selective precipitation is a well-known post-synthetic treatment to isolate nanoparticles of different sizes from each other.[46] We used this technique to purify particles having individual anisotropic shapes from the crude ZAIS particle mixture. ZAIS particles modified with DDT were uniformly dispersed in chloroform, not in methanol, in this study. Thus, the particles enriched with rod-shaped particles were precipitated by the addition of a small amount of methanol acting as a non-solvent in the chloroform solution containing the crude particle mixture, while the supernatant contained a larger fraction of rice-shaped particles than before. By repeating these procedures, typically 3 or 4 times, purified particles having rod or rice shapes were isolated as shown in **Fig. 1e and f,** respectively. The purified particles of each shape had a size similar to that of corresponding particles in the crude mixture.

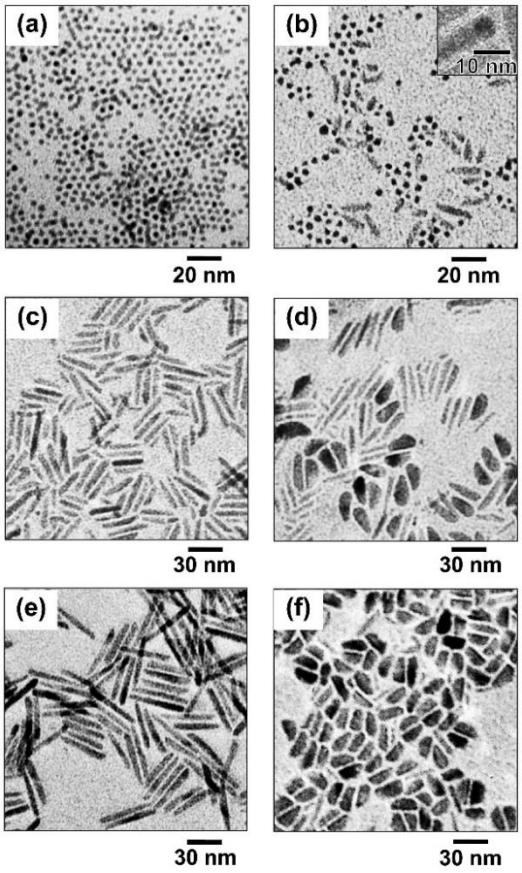

Figure 1. TEM images of nanoparticles produced by the first heating step (150 °C) (a) and those obtained by heating at 250 °C for 1.5 (b), 3.0 (c), and 10 min (d-f) in the second heating process. The metal precursor ratio, x_P, was fixed to 0.50. The particles in panel d, obtained just after heat treatment for 10 min, were subjected to size-selective precipitation to isolate particles of rod (e) and rice shapes (f).

Figure 2 shows XRD patterns of thus-obtained ZAIS particles with rod-like and rice-like shapes. Each pattern agreed well with that expected from the hexagonal wurtzite crystal structure of ZnS-$AgInS_2$ solid solution,[12] while there was no secondary crystal phase, such as Ag_2S or other sulfides. The individual peaks observed in rice-shaped ZAIS particles were shifted to lower diffraction angles than the corresponding peaks of rod-shaped particles, indicating that the lattice constant of rice particles was larger than that of rod particles due to the smaller fraction of ZnS in the ZAIS solid solution. This was confirmed by elemental analysis of obtained ZAIS particles: The ratios of

Ag:In:Zn in the particles were 0.41 : 0.41 : 0.18 and 0.16 : 0.19 : 0.65 for rice particles and rod particles, respectively.

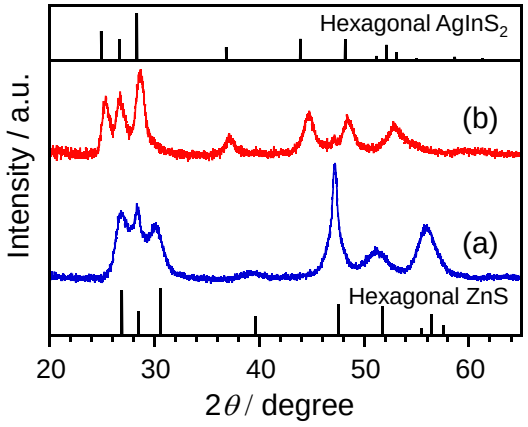

Figure 2. XRD patterns of purified ZAIS particles with (a) rod and (b) rice shapes obtained by size-selective precipitation. ZAIS particles were prepared with x_p = 0.50 by heating at 250 °C for 10 min in the second heating step. XRD patterns of bulk materials are also shown for hexagonal ZnS (PDF# 00-010-043) and hexagonal $AgInS_2$ (PDF# 01-089-502).

Controlling the composition of rod-shaped ZAIS particles by the metal precursor ratio

The chemical composition of ZAIS solid solution is a key factor for controlling the optical properties of resulting particles because their energy gap (E_g) is dependent on their composition. As reported in our previous paper,[29] the composition of spherical ZAIS particles was tunable, with the Ag:In:Zn ratio of resulting particles being almost proportional to that of metal precursors used in the preparation. Based on the results of our previous study, we first attempted to vary the chemical composition of anisotropic ZAIS particles by changing the molar ratio of corresponding metal acetates in preparation, x_p. **Figure 3a-c** show TEM images of rod-shaped ZAIS particles with various x_p values, produced at the early stage of the second heating step at 250 °C, as well as in the case of x_p=0.50 in **Fig. 1c**. The duration of the second heating step was slightly varied from

2 to 5 min to prevent contamination with by-product particles, such as spherical Ag_2S particles and rice-shaped ZAIS particles. Thus-obtained rod-shaped particles exhibited XRD patterns exclusively assignable to the wurtzite crystal structure of ZAIS (**Fig. S2**). The dimensions of rod particles were dependent on the x_p value as shown in **Fig. 3d**: With a decrease in the x_p value from 0.7 to 0.3, that is, with an increase in the content of Zn^{2+} in precursors, the average rod length monotonously increased from 27 to 46 nm and the average width was almost constant at 4.6~5.3 nm.

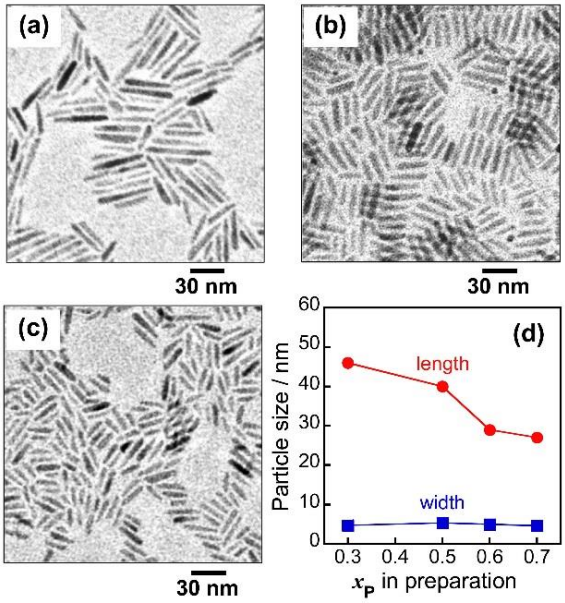

Figure 3. (a-c) TEM images of rod-shaped ZAIS particles obtained by the second heating step at 250 °C for 3~5 min. The x_p values used were 0.30 (a), 0.60 (b) and 0.70 (c). (d) Dependence of the dimensions of ZAIS rods on the metal precursor ratio, x_p.

It is notable that prolonged heat treatment at 250 °C up to 10 min in the second step resulted in production of rice-shaped particles as a by-product at any x_p value in preparation as shown in **Fig. S3**. Their average length was slightly reduced from ca. 19 nm to 14 nm with an increase in x_p from 0.3 to 0.9. Furthermore, the fraction of rod-like particles was remarkably decreased from 91% to

51% by changing the x_p value from 0.3 to 0.8, as shown in **Fig. S3f**. Rice-shaped particles were predominantly formed with relatively large fractions of Ag^+ and In^{3+}, such as x_p = 0.9 and 1.0, being similar to the results of previous studies in which $AgInS_2$ particles with a seed-like shape were produced via a single-step heating-up strategy.[47-48]

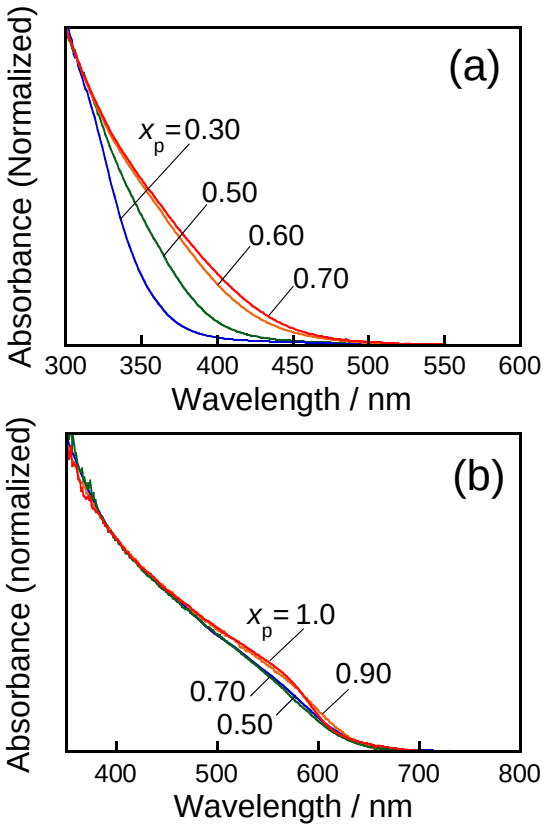

Figure 4. Absorption spectra of (a) rod-shaped ZAIS particles and (b) rice-shaped ZAIS particles prepared with various values of the precursor ratio, x_p. The samples of rod particles were the same as those shown in Fig. 3, while the rice-shaped ZAIS particles were isolated from the crude particle mixtures obtained with the second heating step for 10 min (Fig. S3). The ZAIS particles were uniformly dispersed in chloroform. The numbers in the figure are the precursor ratios.

Figure 4a shows absorption spectra of the rod-shaped ZAIS particles shown in **Fig. 3**. The absorption spectra of rod particles were red-shifted with an increase in the precursor ratio of x_p, indicating that their energy gap was tunable depending on the x_p value used. On the other hand, as

shown in **Fig. 4b**, little change was observed in the absorption spectra of rice-shaped ZAIS particles, which were isolated from the crude particle mixtures (**Fig. S3**) prepared with various x_p values via the second heating step for 10 min, though the amount of rice-shaped particles isolated was too small to measure their absorption spectra in the case of x_p being less than 0.30.

Table 1. Chemical composition of resulting $(AgIn)_xZn_{2(1-x)}S_2$ nanoparticles with rod and rice shapes.

shape	heating duration / min	precursor ratio x_p	composition of particle Ag : In : Zn	x in chemical formula[a]
rod	5	0.30	0.05 : 0.07 : 0.88	0.11
	3	0.50	0.12 : 0.13 : 0.75	0.24
	2.5	0.60	0.14 : 0.15 : 0.71	0.29
	2	0.70	0.19 : 0.17 : 0.64	0.35
rice[b]	10	0.50	0.41 : 0.41 : 0.18	0.82
	10	0.70	0.41 : 0.38 : 0.21	0.79
	10	0.90	0.46 : 0.42 : 0.12	0.88
	10	1.0	0.51 : 0.49 : 0	1.0

[a]The value was calculated from experimentally obtained chemical composition.
[b]The particles were purified by the size selective precipitation.

Table 1 shows the chemical composition of anisotropic-shaped ZAIS particles. Each kind of particle had a nearly stoichiometric ratio of Ag:In:Zn as expected from the ZnS-$AgInS_2$ solid solution regardless of the particle shape. Thus, we could calculate the x value in the composition formula, $(AgIn)_xZn_{2(1-x)}S_2$, for each kind of particle by using the equation $x = (Ag^+ + In^{3+})/(Ag^+ + In^{3+} + Zn^{2+})$. The x value of rod-shaped ZAIS particles increased from 0.11 to 0.35 with an increase in the precursor ratio of x_p from 0.30 to 0.70. On the other hand, the rice-shaped particles, isolated through size-selective precipitation, showed a constant x value of ca. 0.8~0.9, except for the case of the absence of Zn^{2+} in metal precursors, x_p =1.0. Consequently, it was concluded that rice-shaped ZAIS particles, produced after the rod-shaped particles, had an almost

constant composition with a large fraction of $AgInS_2$ that could not be controlled by the metal precursor ratio.

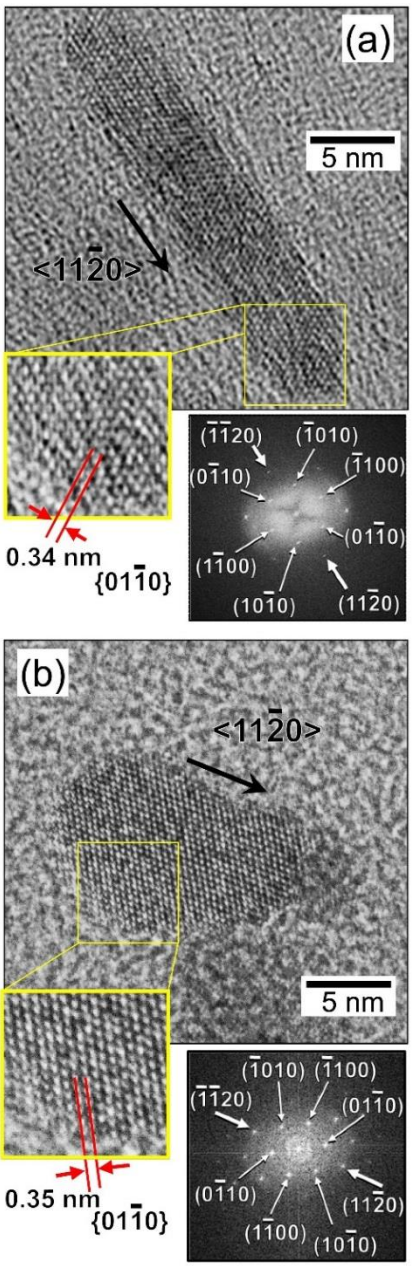

Figure 5. Representative HR-TEM images of (a) rod- and (b) rice-shaped ZAIS particles. The corresponding FFT patterns are indicated in the insets of individual panels.

Mechanism by which anisotropic-shaped ZAIS particles are formed

Figure 5 shows HR-TEM images of rod-shaped ZAIS particles prepared with the precursor ratio of x_p =0.60 (**Fig. 3b**) and rice-shaped particles prepared with x_p = 0.90 (**Fig. S3d**). Continuous lattice fringes were observed throughout the particles, and no grain boundary could be recognized inside the particles regardless of the particle shape, indicating that both rod-shaped particles and rice-shaped particles were comprised of a single crystal of ZnS-$AgInS_2$ solid solution. The rod-shaped ZAIS particle exhibited a lattice fringe with interplanar spacing of 0.34 nm, which was consistent with the (01-10) lattice spacing, 0.337 nm, of a hexagonal crystal structure determined from the XRD pattern of the same rod-shaped particles as those shown in **Fig. S2**. The fast Fourier transform (FFT) pattern of the TEM image exhibited 6-fold symmetry as shown in the inset of **Fig. 5a**, indicating that the incident electron beam was normal to the {0001} plane of the wurtzite crystal. Furthermore, spots corresponding to (-1-120) and (11-20) planes appeared in the same direction of the long axis of the rod particle. It was thus found that the preferential crystal growth of the ZAIS rod was along the <11-20> direction and that the short axis of the rod particle was parallel to <1-100>. Similar anisotropic crystal growth has been reported for several kinds of metal sulfide semiconductors with a hexagonal crystal structure, such as ZnS,[49] $AgInS_2$,[50], ZnS-$AgInS_2$ alloy[51-52], $CuInS_2$[53], and $Cu_xGa_{1-x}S_2$ alloy[53]: Rod-shaped nanoparticles or nanoribbons were often formed with the long axis parallel to <11-20> when these metal sulfide semiconductors were epitaxially grown on initially produced nanocrystals of binary metal chalcogenides, such as silver sulfide[49] and copper sulfide,[53] acting as nuclei. On the other hand, the rice-shaped particle in the HR-TEM image exhibited a clear lattice fringe with interplanar spacing of 0.35 nm, which agreed with the lattice spacing of (01-10) planes, 0.351 nm, determined from XRD patterns for rice-shaped particles with x_p = 0.90. FFT analysis of the HR-TEM image shown in the inset of **Fig. 5b**

revealed that the long axis of the rice-shaped ZAIS crystal was parallel to the <11-20> direction, the crystal growth direction being the same as that of rod-shaped particles.

We propose the formation mechanism of rod-shaped and rice-shaped particles in the two-step heating process as shown in **Fig. 6**. In the first heating step at 150 °C, spherical Ag_2S particles are formed by dominant decomposition of elemental sulfur in the sulfur precursor mixture, since the reactivity of elemental sulfur is higher than that of DBTU.[43] It was reported by Xu et al.[49] that Ag_2S particles not only exhibited a catalytic function for epitaxial growth of a rod-like ZnS nanocrystal on their particle surface via incorporation of Zn^{2+} into the Ag_2S crystal but also acted as a sacrificial source and host for the deposition of $AgInS_2$ rod particles: the Ag_2S crystal was consumed by epitaxial growth of the $AgInS_2$ crystal through diffusion of Ag^+ at the Ag_2S-$AgInS_2$ interface because the high ionic conductivity of the Ag_2S crystal[56-57] enabled metal cations to be incorporated from solution phase into nanoparticles via diffusion in the S sublattice of the Ag_2S crystal. Being similar to these previous studies for multinary metal chalcogenide particles, Ag_2S nanoparticles must be a key material for the crystal growth. When the reaction temperature is raised to 250 °C to decompose DBTU in the sulfur precursor mixture, ZAIS rod crystals start to grow on Ag_2S particles. Some Ag_2S particles act as a source and host for the deposition of ZAIS rod particles, and the other particles are decomposed into individual ions homogeneously re-dissolved in the solution, resulting in the exclusive formation of rod particles at the early stage in the second heating step. The ZAIS rods are elongated with prolongation of heating in the second step until the Zn^{2+} concentration in the solution becomes too small for the concentration of crystal growth of Zn^{2+}-rich ZAIS rods. Finally, rice-shaped particles are deposited via homogeneous nucleation with the use of the remaining Ag^+ and In^{3+} ions in the solution, so that the chemical

composition of as-prepared rice-shaped particles becomes Ag- and In-rich, being difficult to be controlled by variation of the metal precursor ratio, x_p (**Table 1**).

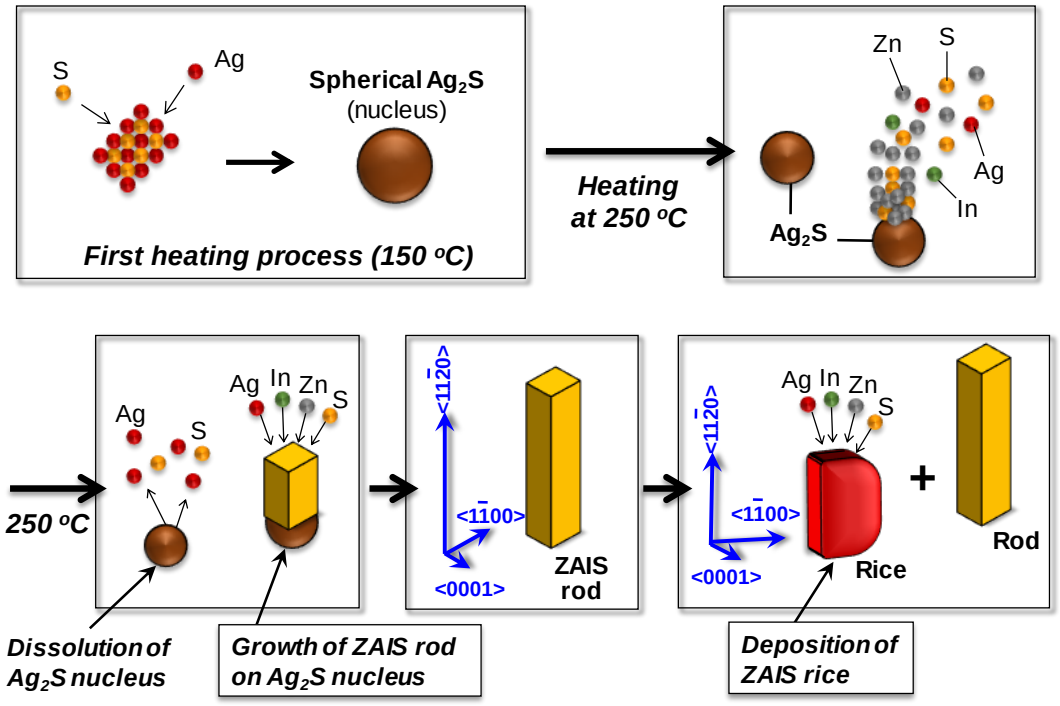

Figure 6. Schematic illustration of the formation of rod- and rice-shaped ZAIS particles.

Zn^{2+} doping of rice-shaped ZAIS particles for tuning chemical composition

Metal cation doping has been used as a post-preparative method to modify the composition of nanoparticles. For example, Zn^{2+} doping into spherical I-III-VI_2 particles of $AgInS_2$[58-59] or $CuInS_2$[60-61] enlarged E_g of resulting particles. Thus, we carried out Zn^{2+} doping of rice-shaped ZAIS particles prepared with x_p= 0.90. Elemental analysis (**Table 2**) revealed that the fraction of Zn^{2+} in rice-shaped ZAIS particles was increased with an increase in the amount of $Zn(CH_3COO)_2$ added to the solution, R_{Zn}, with the x value of rice-shaped particles being controlled from 0.92 to

0.25. **Figure 7a** shows XRD patterns of rice-shaped ZAIS particles with various *x* values obtained by Zn^{2+} doping. The particles had a hexagonal wurtzite crystal structure, with each diffraction peak being shifted to a higher angle with a decrease in *x* as expected from the formation of a homogeneous solid solution. The absorption spectra of thus-obtained particles uniformly dispersed in chloroform were monotonously blue-shifted with an increase in the *x* value as shown in **Fig. 7b**, the onset wavelength being varied from ca. 650 to 500 nm. TEM measurement revealed that Zn^{2+} doping of rice-shaped ZAIS particles was successfully carried out without considerable modification of particle morphology as shown in the inset of **Fig. 7b** and **Fig. S4**: the particles had an average width of ca. 9 nm and average length of ca. 16 nm regardless of R_{Zn} values used for doping. Consequently, E_g of rice-shaped ZAIS particles was successfully controlled by post-preparative Zn^{2+} doping without significant change in the particle morphology.

Table 2. Chemical composition of Zn^{2+}-doped ZAIS nanoparticles with a rice shape.

shape	R_{Zn} [a]	width (nm) × length (nm)	composition of particle Ag : In : Zn	*x* in chemical formula[b]
rice[c]	0	8.8 × 16	0.47 : 0.45 : 0.08	0.92
	0.50	8.9 × 15	0.37 : 0.35 : 0.28	0.72
	1.0	9.4 × 17	0.27 : 0.36 : 0.37	0.63
	1.5	9.0 × 16	0.21 : 0.23 : 0.56	0.45
	2.0	8.2 × 15	0.15 : 0.24 : 0.61	0.39
	2.5	9.1 × 16	0.12 : 0.13 : 0.75	0.25

[a]Molar ratio of $Zn(CH_3COO)_2$ added to OLA to that of total metal ions contained in ZAIS particles used.
[b]The value was calculated from experimentally obtained chemical composition.
[c]Rice-shaped ZAIS particles prepared with x_P= 0.90 were used as starting nanoparticles.

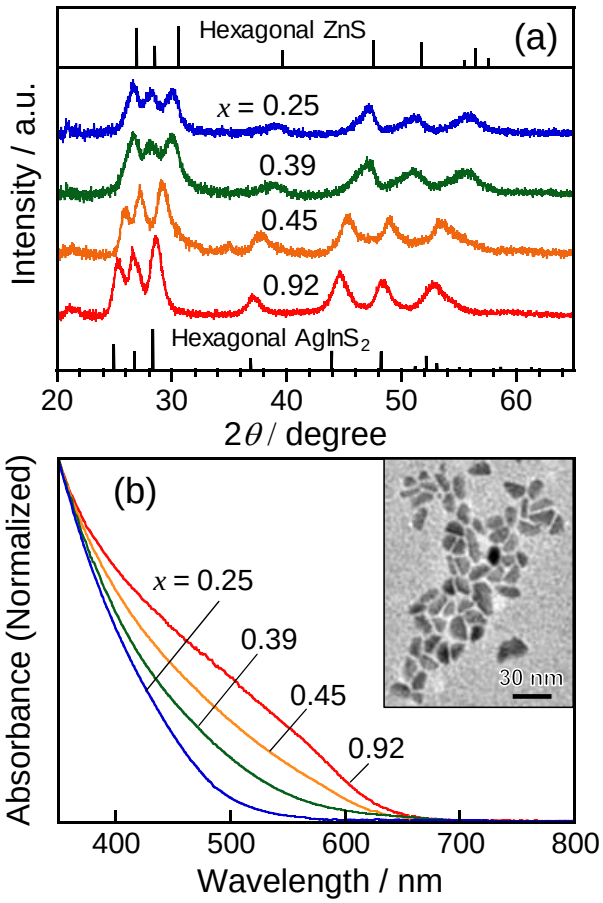

Figure 7. XRD patterns (a) and absorption spectra (b) of Zn^{2+}-doped ZAIS particles with a rice shape. (Inset) A TEM image of Zn^{2+}-doped ZAIS nanoparticles with x= 0.45.

Photocatalytic activity of ZAIS particles depending on the particle shape and chemical composition

In order to avoid contamination of differently shaped particles, we used rod-shaped ZAIS particles, which were prepared by heating at 250 °C for 2~5 min in the early stage of the second heating step (**Fig. 3 and 4a**), and rice-shaped particles for which the chemical composition was controlled by Zn^{2+}-doping (**Fig. 7b and S4**). E_g of anisotropic-shaped ZAIS particles was determined by extrapolating the linear region of Tauc plots (**Fig. S5**) of absorption spectra for

direct transition semiconductors, and it is plotted in **Fig. 8** as a function of the *x* value obtained from elemental analysis. The figure also shows E_g of spherical ZAIS particles of ca. 5.5 nm in diameter used for comparison, which were prepared according to the method reported in our previous paper.[29] With a decrease in the *x* value, E_g of ZAIS particles was monotonously enlarged regardless of the particle shape. The rod-shaped particles showed exceptionally larger E_g than did particles of sphere and rice shapes even if the difference in chemical composition was taken into consideration. According to previous reports that E_g of size-quantized rod-shaped particles is predominantly determined by the short axis,[1, 62] the enlargement of E_g observed for the rod-shaped particles resulted from the quantum size effect: The width of rod-shaped particles (4.6~5.3 nm) was small enough to show the E_g increase, since ZAIS particles with sizes of less than ca. 7~8 nm showed a remarkable quantum size effect.[29]

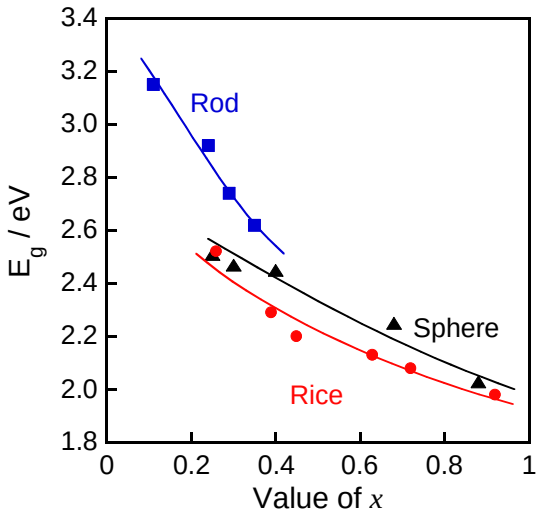

Figure 8. Relationship between E_g and *x* value of ZAIS particles with various shapes.

The anisotropic-shaped ZAIS particles obtained in the present study are suitable materials for

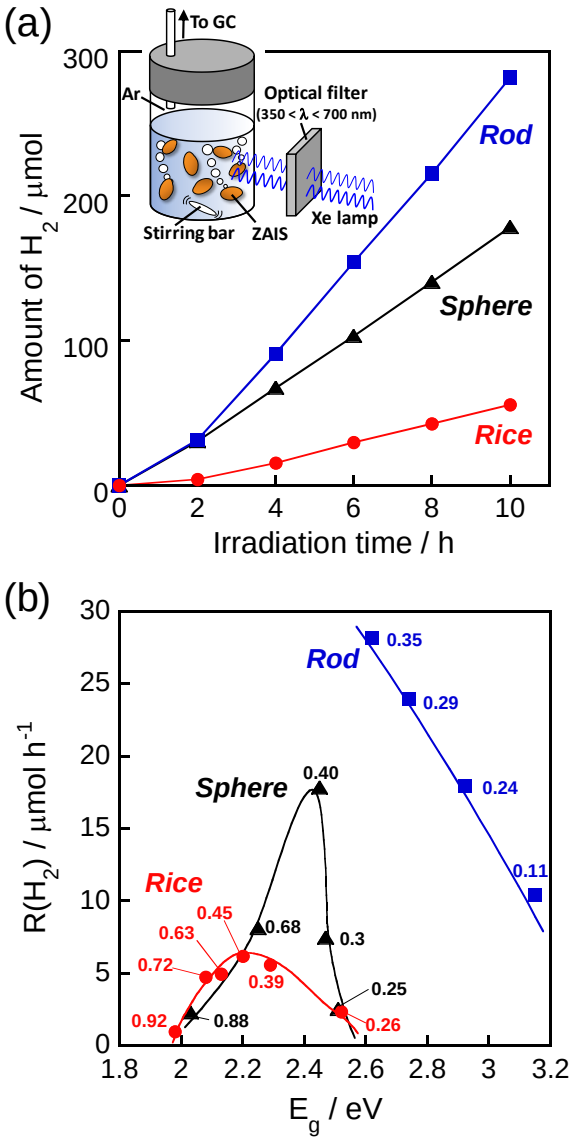

Figure 9. (a) Time courses of H_2 evolution by irradiation of ZAIS particles with rod (x= 0.35), sphere (x= 0.40), and rice (x= 0.45) shapes. The ZAIS particle photocatalysts were dispersed in a water/2-propanol solution containing S^{2-} as a sacrificial electron donor. (Inset) Schematic illustration of the reaction apparatus for photocatalytic H_2 evolution. (b) Relationship between $R(H_2)$ and x value of ZAIS particles with various shapes: rod (squares), sphere (triangles), and rice (circles). The numbers in panel b represent the x values.

investigating the effects of both particle morphology and chemical composition on photocatalytic activities because the methods used for preparation enabled the control of chemical composition

without a significant change in particle morphology. **Figure 9a** shows time courses of the amount of H_2 evolution by irradiation to ZAIS particles having similar *x* values, 0.35~0.45. Linear relations were observed between the amount of H_2 evolved and irradiation time, except for the initial stage of irradiation. After 10 h of irradiation to rod-shaped ZAIS particles shown in **Fig. 9a**, the total amount of evolved H_2 reached ca. 280 μmol, which exceeded the molar amount of ZAIS particles used, 4.5 μmol, by more than 60 times. Furthermore, H_2 evolution at a similar rate was observed repeatedly with Xe lamp irradiation even after the ZAIS particle suspension had been purged with pure Ar gas every 15 h, as shown in **Fig. S6**. These results indicated that H_2 evolution proceeded photocatalytically with irradiation to ZAIS particles. The H_2 evolution rate, $R(H_2)$, was determined from the slope of the linear time course and is plotted in **Fig. 9b** as a function of E_g of ZAIS particles with individual shapes. $R(H_2)$ remarkably varied depending on the morphology of ZAIS particles. Volcano-type dependence was observed for both spherical and rice-shaped particles, with maximum $R(H_2)$ values appearing at E_g of ca. 2.4 and 2.2 eV, respectively. These behaviors were explained by the change in the electronic energy structure of ZAIS particles as reported in our previous paper.[29] The conduction band edge potential (E_{CB}) was sufficiently negative to reduce H^+ to H_2 regardless of their solid solution composition, and then the driving force for H^+ reduction was increased by the negative shift of E_{CB} with a decrease in the *x* value, that is, with an increase in E_g of ZAIS particles.[12, 29] On the other hand, the number of photons absorbed by ZAIS particles became smaller with increase in E_g. The balance of these two factors resulted in the optimal E_g of similar values for spherical and rice-shaped ZAIS nanoparticles, ca. 2.2~2.4 eV. On the other hand, rod-shaped particles exhibited much higher photocatalytic activity; $R(H_2)$ became highest at E_g of 2.6 eV and was monotonously reduced with an increase in E_g. The rod-shaped ZAIS particles should have similar volcano-type dependence at $E_g < 2.6$ eV, though the present method did not

allow us to synthesize them in such an energy gap region. The optimal value of $R(H_2)$ was significantly dependent on the particle morphology and increased in the order of rice < sphere < rod shapes. The apparent quantum yields (AQYs) for photocatalytic H_2 evolution were evaluated with ZAIS particles of optimal *x* value by irradiation of monochromatic light with a wavelength at 400 nm. The ZAIS particles exhibited relatively high activity without loading of a co-catalyst such as Pt, Rh, or Ru nanoparticles: AQYs were 2.0% for rice-shaped particles with x= 0.45, 2.6% for spherical particles with x= 0.40, and 5.9% for rod-shaped particles with x= 0.35.

An understanding of carrier dynamics in ZAIS particles is useful for the elucidation of how the photocatalytic activity of rod-shaped particles was improved. **Figure 10a** shows steady-state PL spectra of ZAIS particles exhibiting the optimal photocatalytic activity of particles with each shape. Broad PL peaks, which were attributed to donor−acceptor pair (DAP) radiative recombination of photogenerated charge carriers or the emission via defect sites, were observed regardless of the particles shape, being similar to those previously reported for spherical ZAIS particles with various compositions.[29, 63-66] The PL peak wavelength of rod particles was the same as that of spherical particles, 572 nm, but the rice-shaped particles having the smallest E_g of the three kinds of particles exhibited a PL peak at a longer wavelength of 645 nm.

PL decay curves of ZAIS particles, measured at corresponding peak wavelengths as shown in **Fig. 10b**, were remarkably varied by the shape of particles used. Each curve could be fitted well with a double-exponential decay function (eq.1) with the fitting parameters listed in **Table S1**:

$$I(t) = A_1 \exp(-t / \tau_1) + A_2 \exp(-t / \tau_2) , \qquad \text{--- (1)}$$

where τ_1 and τ_2 represent the lifetimes of PL emission, and A_1 and A_2 are the amplitudes corresponding to the lifetimes. The average lifetime of PL ($<\tau>$) was calculated using the equation

$\langle\tau\rangle = \Sigma A_i\tau_i^2/\Sigma A_i\tau_i$. Relatively long PL lifetimes, a few hundred nanoseconds or longer, were

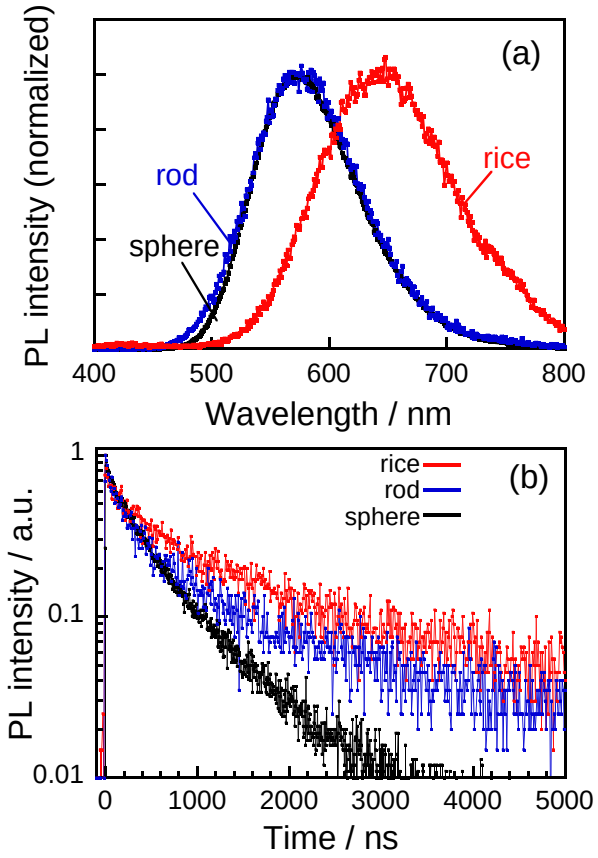

Figure 10. Steady-state PL spectra (a) and PL decay profiles at peak wavelengths (b) of ZAIS particles with rod (x= 0.35), sphere (x= 0.40), and rice (x= 0.45) shapes. The particles were uniformly dispersed in chloroform. The excitation wavelength was 365 nm.

observed, being in accordance with those reported for the DAP recombination in I-III-VI_2 semiconductor nanoparticles.[67-70] Although the faster decay component had a roughly constant lifetime of 200~350 ns, the slower decay component had much longer lifetimes in the range of ca.700~2100 ns, being significantly varied by the shape of ZAIS particles. The average PL lifetime of ZAIS particles increased with the shape in order of sphere (602 ns) < rod (1150 ns) < rice (1730 ns). This is almost acceptable considering the particle volumes of the three samples, i.e., sphere (5.5 nm), rod (4.6 × 27 nm), and rice (9 × 16 nm), where the confinement of charge carriers decreased in the same order. Since the probability for H^+ reduction on ZAIS particles is reasonably

assumed to be enhanced with an increase in the lifetime of electrons photogenerated in the particles, the difference in PL lifetime between rod-shaped and spherical particles can explain the behavior of the former showing larger photocatalytic activity than that of the latter. However the rice-shaped ZAIS particles exhibited the smallest photocatalytic activity for H_2 evolution of the photocatalysts investigated in this study despite exhibiting the longest carrier lifetime. This was probably because rice-shaped particles had deeper trap sites originating from the difference in the preparation processes. Since the lattice constant of a ZAIS crystal decreases with an increase in the Zn fraction, the Zn^{2+}-doping process can induce strain on host ZAIS nanocrystals, resulting in the formation of deeper defect sites in Zn^{2+}-doped particles than in ZAIS particles directly grown from the solution phase.

Conclusion

The two-step heating process with two kinds of sulfur precursors enabled preparation of ZAIS nanoparticles with well-controlled anisotropic shapes, rod shape and rice shape. The chemical composition, which was a factor determining E_g of ZAIS particles, could be controlled without significant change in the particle size and shape: Rod-shaped ZAIS particles had a chemical composition that was tunable by the ratio of corresponding metal acetates used in the preparation, while post-preparative Zn^{2+} doping into rice-shaped particles was necessary to increase the ZnS fraction in the ZAIS solid solution. The morphology of ZAIS particles, as well as the solid solution composition, strongly influenced the photocatalytic activity for H_2 evolution, which reached a maximum at a similar composition of x= 0.35~0.45. The quantum yield for photocatalytic H_2 evolution was significantly enlarged with particle shapes in the order of rice < sphere < rod, with

the rod-shaped ZAIS particles showing activity about two-times larger than that of spherical particles. It was reported in our previous paper[29] that the optical and photochemical properties of multinary semiconductor nanoparticles were controllable depending on their size and chemical composition. In addition to these factors, the results of this study showed that particle shape is another important factor for precisely tuning physicochemical properties of multinary particles. Further development of procedures for synthesis of multinary semiconductor particles having different shapes will provide a novel strategy for improving the efficiency of nanoparticle-based light energy conversion systems such as solar cells and photocatalysts.

ASSOCIATED CONTENT

Supporting Information. The Supporting Information is available free of charge on the ACS Publications website at DOI: Additional figures and table about characterizations of ZAIS particles.

AUTHOR INFORMATION

Corresponding Authors

*E-mail (T. Torimoto): torimoto@apchem.nagoya-u.ac.jp

*E-mail (T. Shibayama): shiba@ufml.caret.hokudai.ac.jp

ACKNOWLEDGMENT

This work was partially supported by JSPS KAKENHI Grant Numbers JP15H00870 and JP15H00863 in Scientific Research on Innovative Areas “Artificial Photosynthesis”, JP16H06507 in Scientific Research on Innovative Areas “Nano-Material Optical-Manipulation”, JP15H03876, and JP16H06052. High-resolution TEM measurements were conducted in Hokkaido University, supported by the Nanotechnology Platform Program of the Ministry of Education, Culture, Sports, Science and Technology (MEXT), Japan. The authors thank Professor Satoshi Minakata and Professor Youhei Takeda (Osaka University) for the PL decay measurements.

REFERENCES

(1) Li, L. S.; Hu, J. T.; Yang, W. D.; Alivisatos, A. P. Band Gap Variation of Size- and Shape-Controlled Colloidal CdSe Quantum Rods *Nano Lett.* **2001**, *1*, 349-351.

(2) Huynh, W. U.; Dittmer, J. J.; Alivisatos, A. P. Hybrid Nanorod-Polymer Solar Cells *Science* **2002**, *295*, 2425-2427.

(3) Grzelczak, M.; Perez-Juste, J.; Mulvaney, P.; Liz-Marzan, L. M. Shape Control in Gold Nanoparticle Synthesis *Chem. Soc. Rev.* **2008**, *37*, 1783-1791.

(4) Chen, H. C.; Lai, C. W.; Wu, I. C.; Pan, H. R.; Chen, I. W. P.; Peng, Y. K.; Liu, C. L.; Chen, C. H.; Chou, P. T. Enhanced Performance and Air Stability of 3.2% Hybrid Solar Cells: How the Functional Polymer and CdTe Nanostructure Boost the Solar Cell Efficiency *Adv. Mater.* **2011**, *23*, 5451-5455.

(5) Tongying, P.; Plashnitsa, V. V.; Petchsang, N.; Vietmeyer, F.; Ferraudi, G. J.; Kryloya, G.; Kuno, M. Photocatalytic Hydrogen Generation Efficiencies in One-Dimensional CdSe Heterostructures *J. Phys. Chem. Lett.* **2012**, *3*, 3234-3240.

(6) Kolny-Olesiak, J.; Weller, H. Synthesis and Application of Colloidal $CuInS_2$ Semiconductor Nanocrystals *ACS. Appl. Mater. Interfaces* **2013**, *5*, 12221-12237.

(7) Weng, B.; Liu, S. Q.; Tang, Z. R.; Xu, Y. J. One-Dimensional Nanostructure Based Materials for Versatile Photocatalytic Applications *RSC Adv.* **2014**, *4*, 12685-12700.

(8) Simon, T.; Bouchonville, N; Berr1, M. J.; Vaneski, A.; Adrovic, A.; Volbers, D.; Wyrwich, R.; Döblinger, M.; Susha, A. S.; Rogach, A. L.; Jäckel1, F.; Stolarczyk, J. K.; Feldmann, J. Redox Shuttle Mechanism Enhances Photocatalytic H_2 Generation on Ni-Decorated CdS Nanorods *Nat. Mater.* **2014**, *13*, 1013-1018.

(9) Li, J. T.; Wu, N. Q. Semiconductor-Based Photocatalysts and Photoelectrochemical Cells for Solar Fuel Generation: a Review *Catal. Sci. Technol.* **2015**, *5*, 1360-1384.

(10) Lang, D.; Xiang, Q. J.; Qiu, G. H.; Feng, X. H.; Liu, F. Effects of Crystalline Phase and Morphology on the Visible Light Photocatalytic H_2 Production Activity of CdS Nanocrystals *Dalton T* **2014**, *43*, 7245-7253.

(11) Wang, X. X.; Liu, M. C.; Zhou, Z. H.; Guo, L. J. Toward Facet Engineering of CdS Nanocrystals and Their Shape-Dependent Photocatalytic Activities *J. Phys. Chem. C* **2015**, *119*, 20555-20560.
(12) Tsuji, I.; Kato, H.; Kobayashi, H.; Kudo, A. Photocatalytic H_2 Evolution Reaction from Aqueous Solutions Over Band Structure-Controlled $(AgIn)_xZn_{2(1-x)}S_2$ Solid Solution Photocatalysts with Visible-Light Response and Their Surface Nanostructures *J. Am. Chem. Soc.* **2004**, *126*, 13406-13413.
(13) Panthani, M. G.; Akhavan, V.; Goodfellow, B.; Schmidtke, J. P.; Dunn, L.; Dodabalapur, A.; Barbara, P. F.; Korgel, B. A. Synthesis of $CuInS_2$, $CuInSe_2$, and $Cu(In_xGa_{1-x})Se_2$ (CIGS) Nanocrystal "Inks" for Printable Photovoltaics *J. Am. Chem. Soc.* **2008**, *130*, 16770-16777.
(14) Guo, Q. J.; Hillhouse, H. W.; Agrawal, R. Synthesis of Cu_2ZnSnS_4 Nanocrystal Ink and Its Use for Solar Cells *J. Am. Chem. Soc.* **2009**, *131*, 11672-11673.
(15) Riha, S. C.; Parkinson, B. A.; Prieto, A. L. Solution-Based Synthesis and Characterization of Cu_2ZnSnS_4 Nanocrystals *J. Am. Chem. Soc.* **2009**, *131*, 12054-12055.
(16) Steinhagen, C.; Panthani, M. G.; Akhavan, V.; Goodfellow, B.; Koo, B.; Korgel, B. A. Synthesis of Cu_2ZnSnS_4 Nanocrystals for Use in Low-Cost Photovoltaics *J. Am. Chem. Soc.* **2009**, *131*, 12554-12555.
(17) Zhong, H. Z.; Bai, Z. L.; Zou, B. S. Tuning the Luminescence Properties of Colloidal I-III-VI Semiconductor Nanocrystals for Optoelectronics and Biotechnology Applications *J. Phys. Chem. Lett.* **2012**, *3*, 3167-3175.
(18) Kim, I; Kim, K.; Oh, Y.; Woo, K.; Cao, G.; Jeong, S.; Moon, J. Bandgap-Graded $Cu_2Zn(Sn_{1-x}Ge_x)S_4$ Thin-Film Solar Cells Derived from Metal Chalcogenide Complex Ligand Capped Nanocrystals *Chem. Mater.* **2014**, *26*, 3957-3965.
(19) Santra, P. K.; Nair, P. V.; Thomas, K. G.; Kamat, P. V. $CuInS_2$-Sensitized Quantum Dot Solar Cell. Electrophoretic Deposition, Excited-State Dynamics, and Photovoltaic Performance *J. Phys. Chem. Lett.* **2013**, *4*, 722-729.
(20) Torimoto, T.; Kameyama, T.; Kuwabata, S. Photofunctional Materials Fabricated with Chalcopyrite-Type Semiconductor Nanoparticles Composed of $AgInS_2$ and Its Solid Solutions *J. Phys. Chem. Lett.* **2014**, *5*, 336-347.
(21) Chen, Y. B.; Chuang, C. H.; Lin, K. C.; Shen, S. H.; McCleese, C.; Guo, L. J.; Burda, C. Synthesis and Photoelectrochemical Properties of $(Cu_2Sn)_xZn_{3(1-x)}S_3$ Nanocrystal Films *J. Phys. Chem. C* **2014**, *118*, 11954-11963.
(22) Jara, D. H.; Yoon, S. J.; Stamplecoskie, K. G.; Kamat, P. V. Size-Dependent Photovoltaic Performance of $CuInS_2$ Quantum Dot-Sensitized Solar Cells *Chem. Mater.* **2014**, *26*, 7221-7228.
(23) Sakamoto, M.; Chen, L. H.; Okano, M.; Tex, D. M.; Kanemitsu, Y.; Teranishi, T. Photoinduced Carrier Dynamics of Nearly Stoichiometric Oleylamine-Protected Copper Indium Sulfide Nanoparticles and Nanodisks *J. Phys. Chem. C* **2015**, *119*, 11100-11105.
(24) Regulacio, M. D.; Han, M. Y. Multinary I-III-VI_2 and I_2-II-IV-VI_4 Semiconductor Nanostructures for Photocatalytic Applications *Acc. Chem. Res.* **2016**, *49*, 511-519.
(25) Du, J.; Du, Z. L.; Hu, J. S.; Pan, Z. X.; Shen, Q.; Sung, J. K.; Long, D. H.; Dong, H.; Sun, L. T.; Zhong, X. H., Wan, L.-J. Zn-Cu-In-Se Quantum Dot Solar Cells with a Certified Power Conversion Efficiency of 11.6% *J. Am. Chem. Soc.* **2016**, *138*, 4201-4209.
(26) Takahashi, T.; Kudo, A.; Kuwabata, S.; Ishikawa, A.; Ishihara, H.; Tsuboi, Y.; Torimoto, T. Plasmon-Enhanced Photoluminescence and Photocatalytic Activities of Visible-Light-

Responsive ZnS-$AgInS_2$ Solid Solution Nanoparticles *J. Phys. Chem. C* **2013**, *117*, 2511-2520.

(27) Yu, X. L.; An, X. Q.; Shavel, A.; Ibanez, M.; Cabot, A. The effect of the Ga content on the photocatalytic hydrogen evolution of $CuIn_{1-x}Ga_xS_2$ nanocrystals *J. Mater. Chem. A* **2014**, *2*, 12317-12322.

(28) Yu, X. L.; Shavel, A.; An, X. Q.; Luo, Z. S.; Ibanez, M.; Cabot, A. Cu_2ZnSnS_4-Pt and Cu_2ZnSnS_4-Au Heterostructured Nanoparticles for Photocatalytic Water Splitting and Pollutant Degradation *J. Am. Chem. Soc.* **2014**, *136*, 9236-9239.

(29) Kameyama, T.; Takahashi, T.; Machida, T.; Kamiya, Y.; Yamamoto, T.; Kuwabata, S.; Torimoto, T. Controlling the Electronic Energy Structure of ZnS-$AgInS_2$ Solid Solution Nanocrystals for Photoluminescence and Photocatalytic Hydrogen Evolution *J. Phys. Chem. C* **2015**, *119*, 24740-24749.

(30) Ye , C.; Regulacio, M. D.; Lim, S. H.; Li, S.; Xu, Q. H.; Han, M. Y. Alloyed ZnS-$CuInS_2$ Semiconductor Nanorods and Their Nanoscale Heterostructures for Visible-Light-Driven Photocatalytic Hydrogen Generation *Chem. Eur. J.* **2015**, *21*, 9514-9519.

(31) Prusty, G.; Guria, A. K.; Mondal, I.; Dutta, A.; Pal, U.; Pradhan, N. Modulated Binary-Ternary Dual Semiconductor Heterostructures *Angew. Chem. Int. Ed.* **2016**, *55*, 2705-2708.

(32) Ye, C.; Regulacio, M. D.; Lim, S. H.; Xu, Q. H.; Han, M. Y. Alloyed $(ZnS)_x(CuInS_2)_{(1-x)}$ Semiconductor Nanorods: Synthesis, Bandgap Tuning and Photocatalytic Properties *Chem. Eur. J.* **2012**, *18*, 11258-11263.

(33) Regulacio, M. D.; Ye, C.; Lim, S. H.; Zheng, Y. G.; Xu, Q. H.; Han, M. Y. Facile Noninjection Synthesis and Photocatalytic Properties of Wurtzite-Phase $CuGaS_2$ Nanocrystals with Elongated Morphologies *CrystEngComm* **2013**, *15*, 5214-5217.

(34) Fan, C. M.; Regulacio, M. D.; Ye, C.; Lim, S. H.; Lua, S. K.; Xu, Q. H.; Dong, Z. L.; Xu, A. W.; Han, M. Y. Colloidal Nanocrystals of Orthorhombic Cu_2ZnGeS_4: Phase-Controlled Synthesis, formation mechanism and photocatalytic behavior *Nanoscale* **2015**, *7*, 3247-3253.

(35) Bao, N. Z.; Qiu, X. M.; Wang, Y. H. A.; Zhou, Z. Y.; Lu, X. H.; Grimes, C. A.; Gupta, A. Facile Thermolysis Synthesis of $CuInS_2$ Nanocrystals with Tunable Anisotropic Shape and Structure *Chem. Commun.* **2011**, *47*, 9441-9443.

(36) Ibanez, M.; Cadavid, D.; Anselmi-Tamburini, U.; Zamani, R.; Gorsse, S.; Li, W. H.; Lopez, A. M.; Morante, J. R.; Arbiol, J.; Cabot, A. Colloidal Synthesis and Thermoelectric Properties of Cu_2SnSe_3 Nanocrystals *J. Mater. Chem. A* **2013**, *1*, 1421-1426.

(37) Chang, S. H.; Chiu, B. C.; Gao, T. L.; Jheng, S. L.; Tuan, H. Y. Selective Synthesis of Copper Gallium Sulfide ($CuGaS_2$) Nanostructures of Different Sizes, Crystal Phases, and Morphologies *CrystEngComm* **2014**, *16*, 3323-3330.

(38) Zamani, R. R.; Ibanez, M.; Luysberg, M.; Garcia-Castello, N.; Houben, L.; Prades, J. D.; Grillo, V.; Dunin-Borkowski, R. E.; Morante, J. R.; Cabot, A., Arbiol, J. Polarity-Driven Polytypic Branching in Cu-Based Quaternary Chalcogenide Nanostructures *ACS Nano* **2014**, *8*, 2290-2301.

(39) Zhang, X. Y.; Guo, G. B.; Ji, C.; Huang, K.; Zha, C. Y.; Wang, Y. F.; Shen, L. M.; Gupta, A.; Bao, N. Z. Efficient Thermolysis Route to Monodisperse Cu_2ZnSnS_4 Nanocrystals with Controlled Shape and Structure *Sci. Rep.* **2014**, *4*, 5086.

(40) Singh, S.; Liu, P.; Singh, A.; Coughlan, C.; Wang, J. J.; Lusi, M.; Ryan, K. M. Colloidal $Cu_2ZnSn(SSe)_4$ (CZTSSe) Nanocrystals: Shape and Crystal Phase Control to Form Dots, Arrows, Ellipsoids, and Rods *Chem. Mater.* **2015**, *27*, 4742-4748.

(41) van der Stam, W.; Bladt, E.; Rabouw, F. T.; Bals, S.; Donega, C. D. Near-Infrared Emitting $CuInSe_2/CuInS_2$ Dot Core/Rod Shell Heteronanorods by Sequential Cation Exchange *ACS Nano* **2015**, *9*, 11430-11438.
(42) Kameyama, T.; Ishigami, Y.; Yukawa, H.; Shimada, T.; Baba, Y.; Ishikawa, T.; Kuwabata, S.; Torimoto, T. Crystal Phase-Controlled Synthesis of Rod-Shaped $AgInTe_2$ Nanocrystals for in vivo Imaging in the Near-Infrared Wavelength Region *Nanoscale* **2016**, *8*, 5435-5440.
(43) Nishi, H.; Nagano, T.; Kameyama, T.; Kuwabata, S.; Torimoto, T. Well-Controlled Synthesis of Wurtzite-Type Cu_2ZnSnS_4 Nanoparticles Using Multiple Sulfur Sources via a Two-Step Heating Process *CrystEngComm* **2015**, *17*, 174-182.
(44) Wu, X. J.; Huang, X.; Qi, X. Y.; Li, H.; Li, B.; Zhang, H. Copper-Based Ternary and Quaternary Semiconductor Nanoplates: Templated Synthesis, Characterization, and Photoelectrochemical Properties *Angew. Chem. Int. Ed.* **2014**, *53*, 8929-8933.
(45) Singh, A.; Coughlan, C.; Milliron, D. J.; Ryan, K. M. Solution Synthesis and Assembly of Wurtzite-Derived Cu-In-Zn-S Nanorods with Tunable Composition and Band Gap *Chem. Mater.* **2015**, *27*, 1517-1523.
(46) Murray, C. B.; Norris, D. J.; Bawendi, M. G. Synthesis and Characterization of Nearly Monodisperse CdE (E= S, Se, Te) Semiconductor Nanocrystallites *J. Am. Chem. Soc.* **1993**, *115*, 8706-8715.
(47) Li, X. M.; Niu, J. Z.; Shen, H. B.; Xu, W. W.; Wang, H. Z.; Li, L. S. Shape Controlled Synthesis of Tadpole-Like and Heliotrope Seed-Like $AgInS_2$ Nanocrystals *CrystEngComm* **2010**, *12*, 4410-4415.
(48) Deng, M. J.; Shen, S. L.; Wang, X. W.; Zhang, Y. J.; Xu, H. R.; Zhang, T.; Wang, Q. B. Controlled Synthesis of $AgInS_2$ Nanocrystals and Their Application in Organic-Inorganic Hybrid Photodetectors *CrystEngComm* **2013**, *15*, 6443-6447.
(49) Zhu, G. X.; Xu, Z. Controllable Growth of Semiconductor Heterostructures Mediated by Bifunctional Ag_2S Nanocrystals as Catalyst or Source-Host *J. Am. Chem. Soc.* **2011**, *133*, 148-157.
(50) Liu, Z. P.; Tang, K. B.; Wang, D. K.; Wang, L. L.; Hao, Q. Y. Facile Synthesis of $AgInS_2$ Hierarchical Flowerlike Nanoarchitectures Composed of Ultrathin Nanowires *Nanoscale* **2013**, *5*, 1570-1575.
(51) Yang, X. Y.; Tang, Y. X.; Tan, S. T.; Bosman, M.; Dong, Z. L.; Leck, K. S.; Ji, Y.; Demir, H. V.; Sun, X. W. Facile Synthesis of Luminescent $AgInS_2$-ZnS Solid Solution Nanorods *Small* **2013**, *9*, 2689-2695.
(52) Tang, X. S.; Zang, Z. G.; Zu, Z. Q.; Chen, W. W.; Liu, Y.; Han, G. Q.; Lei, X. H.; Liu, X. M.; Du, X. Q.; Chen, W. M.; Yu Wang, Y; Xue, J. A Facile Method for the Synthesis of Quaternary Ag-In-Zn-S Alloyed Nanorods *Nanoscale* **2014**, *6*, 11803-11809.
(53) Li, Q.; Zhai, L. L.; Zou, C.; Huang, X. S.; Zhang, L. J.; Yang, Y.; Chen, X.; Huang, S. M. Wurtzite $CuInS_2$ and $CuIn_xGa_{1-x}S_2$ Nanoribbons: Synthesis, Optical and Photoelectrical Properties *Nanoscale* **2013**, *5*, 1638-1648.
(54) Bai, T. Y.; Li, C. G.; Li, F. F.; Zhao, L.; Wang, Z. R.; Huang, H.; Chen, C. L.; Han, Y.; Shi, Z.; Feng, S. H. A Simple Solution-Phase Approach to Synthesize High Quality Ternary $AgInSe_2$ and Band Gap Tunable Quaternary $AgIn(S_{1-x}Se_x)_2$ Nanocrystals *Nanoscale* **2014**, *6*, 6782-6789.

(55) Huang, F.; Zhou, J. C.; Xu, J.; Wang, Y. S. Formation of $AgGaS_2$ Nano-Pyramids from Ag_2S Nanospheres through Intermediate Ag_2S-$AgGaS_2$ Heterostructures and $AgGaS_2$ Sensitized Mn^{2+} Emission *Nanoscale* **2014**, *6*, 2340-2344.
(56) Miyatani, S. Y. Electrical Properties of Pseudo-Binary Systems of Ag_2VI's; $Ag_2Te_xSe_{1-X}$, $Ag_2Te_xS_{1-X}$, and $Ag_2Se_xS_{1-X}$ *J. Phys. Soc. Jpn.* **1960**, *15*, 1586-1595.
(57) Ivanov-Shitz, A. K. Computer Simulation of Superionic Conductors: II. Cationic Conductors. Review *Crystallogr. Rep.* **2007**, *52*, 302-315.
(58) Tang, X. S.; Ho, W. B. A.; Xue, J. M. Synthesis of Zn-Doped $AgInS_2$ Nanocrystals and Their Fluorescence Properties *J. Phys. Chem. C* **2012**, *116*, 9769-9773.
(59) Mao, B. D.; Chuang, C. H.; Lu, F.; Sang, L. X.; Zhu, J. J.; Burda, C. Study of the Partial Ag-to-Zn Cation Exchange in $AgInS_2$/ZnS Nanocrystals *J. Phys. Chem. C* **2013**, *117*, 648-656.
(60) De Trizio, L.; Prato, M.; Genovese, A.; Casu, A.; Povia, M.; Simonutti, R.; Alcocer, M. J. P.; D'Andrea, C.; Tassone, F.; Manna, L. Strongly Fluorescent Quaternary Cu–In–Zn–S Nanocrystals Prepared from $Cu_{1-x}InS_2$Nanocrystals by Partial Cation Exchange *Chem. Mater.* **2012**, *24*, 2400-2406.
(61) Perera, S. D.; Zhang, H. T.; Ding, X. Y.; Nelson, A.; Robinson, R. D. Nanocluster Seed-Mediated Synthesis of $CuInS_2$ Quantum Dots, Nanodisks, Nanorods, and Doped Zn-$CuInGaS_2$ Quantum Dots *J. Mater. Chem. C* **2015**, *3*, 1044-1055.
(62) Talaat, H.; Abdallah, T.; Mohamed, M. B.; Negm, S.; El-Sayed, M. A. The Sensitivity of the Energy Band Gap to Changes in the Dimensions of the CdSe Quantum Rods at Room Temperature: STM and Theoretical Studies *Chem. Phys. Lett.* **2009**, *473*, 288-292.
(63) Torimoto, T.; Adachi, T.; Okazaki, K.; Sakuraoka, M.; Shibayama, T.; Ohtani, B.; Kudo, A.; Kuwabata, S. Facile Synthesis of ZnS-$AgInS_2$ Solid Solution Nanoparticles for a Color-Adjustable Luminophore *J. Am. Chem. Soc.* **2007**, *129*, 12388-12389.
(64) Torimoto, T.; Ogawa, S.; Adachi, T.; Kameyama, T.; Okazaki, K. I.; Shibayama, T.; Kudo, A.; Kuwabata, S. Remarkable Photoluminescence Enhancement of ZnS-$AgInS_2$ Solid Solution Nanoparticles by Post-Synthesis Treatment *Chem. Commun.* **2010**, *46*, 2082-2084.
(65) Deng, D. W.; Cao, J.; Qu, L. Z.; Achilefu, S.; Gu, Y. Q. Highly Luminescent Water-Soluble Quaternary Zn-Ag-In-S Quantum Dots for Tumor Cell-Targeted Imaging *Phys. Chem. Chem. Phys.* **2013**, *15*, 5078-5083.
(66) Gabka, G.; Bujak, P.; Giedyk, K.; Ostrowski, A.; Malinowska, K.; Herbich, J.; Golec, B.; Wielgus, I.; Pron, A. A Simple Route to Alloyed Quaternary Nanocrystals Ag-In-Zn-S with Shape and Size Control *Inorg. Chem.* **2014**, *53*, 5002-5012.
(67) Zhong, H. Z.; Lo, S. S.; Mirkovic, T.; Li, Y. C.; Ding, Y. Q.; Li, Y. F.; Scholes, G. D. Noninjection Gram-Scale Synthesis of Monodisperse Pyramidal $CuInS_2$ Nanocrystals and Their Size-Dependent Properties *ACS Nano* **2010**, *4*, 5253-5262.
(68) Mao, B. D.; Chuang, C. H.; Wang, J. W.; Burda, C. Synthesis and Photophysical Properties of Ternary I-III-VI $AgInS_2$ Nanocrystals: Intrinsic versus Surface States *J. Phys. Chem. C* **2011**, *115*, 8945-8954.
(69) Li, L. A.; Pandey, A.; Werder, D. J.; Khanal, B. P.; Pietryga, J. M.; Klimov, V. I. Efficient Synthesis of Highly Luminescent Copper Indium Sulfide-Based Core/Shell Nanocrystals with Surprisingly Long-Lived Emission *J. Am. Chem. Soc.* **2011**, *133*, 1176-1179.
(70) Hamanaka, Y.; Ogawa, T.; Tsuzuki, M.; Ozawa, K.; Kuzuya, T. Luminescence Properties of Chalcopyrite $AgInS_2$ Nanocrystals: Their Origin and Related Electronic States *J. Lumin.* **2013**, *133*, 121-124.

TOC

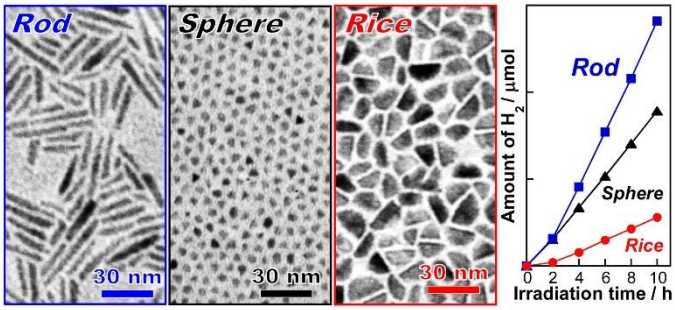
Rod
Sphere
Rice
30 nm
30 nm
30 nm
Amount of H2 / μmol
Rod
Sphere
Rice
0 2 4 6 8 10
Irradiation time / h